Review:

Basement structure of the Hontomin CO$_2$ storage site (Spain) determined by integration of microgravity and 3D seismic data

by Andres et al.

This paper presents a detail gravity model of the study area that incorporates seismic data to constrain the model. The paper is relevant and appropriate for inclusion in Solid Earth with modest revision.

General comments:

(1) Some of the figures need to be redone so that can be more readable in print. The text is too small in some and a larger font will be needed. For instance, Figure for location references along the edge of the Figs. 4a, b, c, and d are unreadable and so the color bar key. Likewise, the stratigraphy key in Figure 5 is unreadable at the scale that I reviewed it at and would not likely be readable in print form at any scale.

(2) Figure 5 should become Figures 5, 6, and 7 and all should have rock type keys.

(3) Figure 11 needs some work. It needs a key and the fault traces need to be clearer. For instance, what is meant by the "Fault" label on the right-side vertical axis versus the dashed lines that are drawn to represent faults? What do the two shades of all the colors mean? Very confusing.

(4)This paper is generally well written but pronouns have been abused. Many of the indefinite "it"s need to be corrected and replaced with the noun that they refer to. Also, you should consider rewriting the any sentence that starts with "There is" and bring the noun to the front. These suggestions will make your meaning more clear.

(5) "Data" is plural.

(6) Lines 6-7: Explain what you mean by "expression". This sentence is unclear.

(7) Lines 28-29: "calculate that of the Triassic" makes no sense. What are you calculating?

(8) Table 1: What are **all** the ages of the formations? I think that you remove the work "Top" from all the Formation names. A formation has a density, not its top.

Below is a scan of my hand-written editorial comments.

Abstract

A multidisciplinary study has been carried out in Hontomín (Spain) to determine the basement structural setting/ geometry and that of the sedimentary succession of an area aimed to be the first Spanish pilot plant of CO_2 injection. An integration of coincident 3D seismic results, borehole data and unpublished microgravity maps aims to reproduce the deep structure of the basement and to quantify the thickness of the Triassic Keuper evaporites. All datasets manage to clearly identify two main fault systems compartmentalizing the main structural domains into three differentiated blocks. These have been interpreted to be reactivated normal faults that have led to the formation of the Hontomín dome. The general structure is characterized by a half-graben setting filled with thick Keuper evaporites (up to 2000m thick) forming an extensional forced fold.

1. Introduction

Gravity data has proven to be useful to model the basement topography in settings where it is overlaid by thick sedimentary successions (e.g. Døssing et al., 2014; Engen, et al., 2006; Chappell et al., 2008). This approach is sensitive to the effective removal of the gravimetric signature of the sedimentary cover and the regional, long wave-length anomaly contribution. Thus, it requires a good knowledge of the sedimentary succession and its configuration in depth. More importantly, the nature of the gravity methods allows a mutual benefit with the seismic method: gravimetric inversion profits from constraints provided by the seismic data since they help to minimize the number of possible solutions, and gravity can aid with the imaging in areas in which the seismic method is less effective, such as in sub-salt areas (e.g., Contrucci et al., 2004; Filina, et al., 2015; Staedtler et al., 2014).

The Hontomín structure was chosen amongst other options (Prado et al., 2008) to encompass the first CO_2 storage Technological Development Plant of Spain. Following the European Union regulation (European Union, 2009) and best practice recommendations from international experts (e.g., IEAGHG, 2008), a multidisciplinary study was carried out to assess its suitability for geological storage of CO_2. This included the implementation of detailed geophysical/petrophysical (Alcalde et al.,

2013a,b; Ogaya et al., 2013, 2014; Ugalde et al., 2013; Vilamajó et al., 2013, Rubio et al., 2011), geomechanical (Canal et al., 2013) and geochemical (Elío et al., 2013; Nisi et al., 2013; Permanyer et al., 2013) characterization methods.

Amongst this multidisciplinary approach, the acquisition, processing and interpretation of a 3D seismic dataset provided the first detailed image of the subsurface of Hontomín (Alcalde et al., 2014). However, seismic data have problems when imaging the subsalt configurations due to the high velocities of salt rock (Rousseau et al., 2003; Sava et al., 2004). The main problem is often the disappearance of the base of the salt or an unclear image of its surface (Leveille et al., 2005). In this context, gravity data can help constraining the contact between the salt and the underlying basement due to the density contrast. The salt has typically very low density (2.16-2.25 kgm^{-3}) while the layers below should have a higher density. This density contrast can be used in order to resolve the geometry of the salt body (Jacoby et al., 2005).

A microgravity survey was carried out in the Hontomin CO_2 storage Technological Development Plant area (Andrés, 2012) with the goal to provide additional constraints to the structure where it was poorly deduced from 3D seismics. Gravity information becomes especially important in this area, where the seismic image is unable to provide enough information in the deepest part of the sedimentary succession and, more importantly, in the basement (Stadtler, et al., 2014). The acquired high resolution data has an excellent quality, providing a complementary approach to unravel the structure of the area. The good control of the sedimentary sequence has allowed us an accurate removal of the sedimentary cover gravity signature from the Bouguer anomaly map in order to focus on the basement structure. The gradients present on the resulting map suggest the existence of important fractures, some of them affecting the basement, that are clearly related with those reported by Alcalde et al., (2013b, 2014). This supports their interpretation and represents a further step in the understanding of the geological evolution of the area. The integration of geophysical datasets presented in this paper is the best contribution to the knowledge of the overall geological structure, of this injection site and a good example of how multidisciplinary high resolution approaches can shed light on the shallow/or deep investigation of geologically complex areas.

2. Geological setting

The Hontomín structure is located within the doubly verging Pyrenean Orogen, in the southeastern part of the Plataforma Burgalesa, to the south of the Mesozoic Basque-Cantabrian Basin (Serrano and Martínez del Olmo, 1990; Tavani, 2012) (Figure 1). This

5   area is characterized by an ESE-dipping monocline bounded to the south by the right-lateral Ubierna Fault System (Tavani et al. 2011) and by the Sierra de Cantabria Thrust to the north. Geographically, it is bounded to the south by the Duero and Ebro basins and to the north by the Sierra de Cantabria.

The Plataforma Burgalesa was affected by three major deformation stages after the

10   Permian period. The first stage corresponds to a Permian-Triassic extension (García-Mondejar et al., 1996) which reactivated wrench-fault systems (Manspeizer,. 1988) giving rise to a set of ESE-WNW and E-W trending normal faults. The second event is related to the continental break-up and opening of the Bay of Biscay (García-Mondejar et al., 1996, Ziegler 1988). This extensional episode triggered the formation of the

15   Basque-Cantabrian basin and the Plataforma Burgalesa. During this deformation episode, NNE-SSW faults were formed almost perpendicularly to the previous fault systems, and the Keuper rocks provided the decoupling surface that ensured different deformation styles between the sedimentary sequences above and the basement below (Tavani and Muñoz, 2012; Tavani et al., 2013). The evaporites themselves were folded

20   with geometries that are diagnostic of extensional forced folds (Brown, 1980; Laubscher, 1982; Tavani et al., 2011, 2013). Finally, the Pyrenean orogeny provided the compressional tectonic setting in which previous faults were reactivated with inverse and lateral offsets (Quintá et al, 2012; Tavani et al., 2011, 2013). Among these, the Ubierna Fault System stands out as the most prominent tectonic feature in the study

25   area. In some places, rocks of similar ages are exposed on both fault walls despite the presence of second-order faults and folds in its southern block. This, together with the well-preserved Mesozoic extensional architecture and with macro- and meso-structural data (Tavani et al., 2011a), highlights an almost exclusive strike-slip behaviour during the Cenozoic inversion stage, with a much subordinated reverse component.

30   The sedimentary succession of the study area (Figure 2) lies over a Palaeozoic basement, and includes a Mesozoic cover topped by Cenozoic sediments. It begins with the Triassic Keuper facies formed by evaporites and anhidrites which are followed by

Lower Jurassic anhidrites and dolomites (Pujalte et al., 2004). Above this, a succession of Lower to Middle Jurassic pelagic and hemipelagic carbonate sediments is found. Following the stratigraphic succession, Purbeck facies of the Late Jurassic-Early Cretaceous formed by clays, carbonates and sandstones lay unconformably above the

5   marine Lower to Middle Jurassic rocks. Up-sequence, a siliciclastic succession is found, comprised by the Weald facies and the Escucha and Utrillas Formations, which are interpreted as fluvial successions with sandstone infilled channels alternating with flood plain sediments. The stratigraphic succession ends up with Upper Cretaceous carbonates and lacustrine and detritic Cenozoic sediments lying unconformably above the

10   Mesozoic series (Vera, 2004).

3. Datasets and Methodology

3.1. Seismic and well data

15   A 3D seismic dataset was acquired in summer 2010 in Hontomín, across an area of 36 km^2 centered according to the target dome-shaped structure (Alcalde et al., 2013a) (Figure 2). The acquired seismic dataset was processed down to 1500 ms up to post-stack time migration (Alcalde et al., 2013b). Critical steps in processing were related to the existence of an unexpected velocity inversion near the surface, which decreased the

20   general quality of the data. However, the final migrated volume provided clear images from the underground structures down to the anhydrite level (i.e., the bottom of the dome structure). Further details on the seismic data acquisition and processing can be found in Alcalde et al. (2013a, b and 2014).

The seismic data was integrated with well-log data from four hydrocarbon exploration

25   boreholes (H1 to H4), and three shallow groundwater sampling wells (GW1 to GW3) (Figure 2). Results indicate that the structure of the Hontomín dome includes eight different sedimentary packages, from Triassic to Cenozoic and four sets of faults. The target Mesozoic dome structure has a NW-SE orientation, and is bounded by two major faults, the South ("S") and the East ("E") faults showing vertical offsets of up to 450

30   and 250 m respectively. Another two sets of faults have been singled out: they trend N-S and E-W respectively and have been related to extensional episodes that occurred during

the opening of the Bay of Biscay. The dips of the dome flanks decrease upwards suggesting a protracted and discontinuous growth. The joint interpretation of the seismic and well log data allowed inferring three evolutionary stages for the Hontomín structure (Alcalde et al., 2104): (1) the development of N-S trending faults as a

5   consequence of differential loading around Triassic E-W faults could have allowed the development of the lowermost Jurassic units and probably produced forced folding of the Hontomín Dome. (2) Later on, the development of E-trending faults during the opening of the Bay of Biscay is recorded by the accumulation of Purbeck deposits. Simultaneously, the migration of the Triassic salts would have further increased the

10   dome's growth. (3) Finally, the Pyrenean Orogeny caused the reactivation of the South and East Faults and the final development of the dome structure.

3.2 Gravity data

Microgravity data was acquired between August and December 2010 by Implemental

15   System Company. A high density mesh covering an area of 4x4 km^2 was recorded, with measurements taken every 100 m, which resulted in 1600 total measured points (Figure 2). The acquisition parameters ensured a resolution lower than 4µGal, with an average above 3 measurements per grid point. 7 gravimetric base stations and 78 control points, with vertical uncertainty of 0.5 cm were constructed.

20   The gravity data was provided without the effects of moon/sun/earth tides and instrumental drift, which were already corrected by the contractor. The data was then processed using GEOSOFT Oasis MontajTM to produce the Bouguer anomaly (BA) map of the area. This includes carrying out the Bouguer slab, free air and terrain corrections (Blakely, 1995). The result, i.e. the Bouguer anomaly map, is shown in

25   Figure 3. The reduction density used was 2400 kg/m^3 since it is the value that shows less correlation between the anomaly map and the topography.

Several procedures may be applied to Bouguer anomaly data in order to enhance features that may later on help in the interpretation. Accordingly, the following processes were carried out in the present dataset: (1) Separation of the long and short

30   wavelength components; (2) Calculation of the gravity derivatives, (vertical and the

total horizontal derivative THD); (3) Construction of two 2D gravity models; (4) Inversion of gravity data.

To carry out a qualitatively assessment of the source depth in the Bouguer Anomaly data, the short and long wavelength number components have to be separated. This

5   separation was performed by applying an upward continuation to the gravity field (Jacobsen, 1987) up to 350 m. This filter was selected in order to minimize distortion and ring effects (Figures 4a and b).

Often, edge enhancements have been used in order to aid the potential field data interpretation (Verduzco, et al. 2004). Accordingly, two sets of derivatives were

10   performed to our dataset aiming to highlight the gradient zones and accordingly, the structural setting of the area. The vertical derivative (Figure 4c) (Blakely and Simpson, 1986) and total horizontal derivative (THD, Figure 4d) show a coherent result between them. Both maps highlight coincident areas with maximum gradient, that is, areas where the contacts between materials of different density exist. However, the vertical

15   derivative also enhances those that are shallow.

Two 2D gravity models were extracted from the Bouguer Anomaly map in order to produce an image of the structure of the area along two profiles (see location in Figure 3): Model 1, striking NE-SW and Model 2 striking almost E-W (Figure 5). First, these models were computed with the assistance of the information provided by wells H1 and

20   H2 but without the input of 3D seismic data (Andrés, 2012) (table 1). The models were then revisited to include the variations in layer's depth and fault's offsets observed in the seismic model (Figure 5a). It is worth highlighting that the changes on the models hence introduced were not significant and provide a good match with the seismic model.

25   **3.3 Gravity inversion**

Gravity data can be inverted in order to obtain the topography of a desired layer (Oldenburg 1974). However, results of inversion are more reliable when the number of variables to invert decrease. Inverting just the topography of one layer can provide us with excellent results if we can preliminary establish the density of every layer and the

30   thickness of every density interval except that of the ones that will be inverted. The

method utilized in this study is based on the Parker's algorithm (Blakely, 1996; Parker, 1972). It works on the frequency domain and is integrated in GM-SYS 3D platform.

The great amount of information available in the Hontomín area has granted us the basis to build a well constrained model that allows us to perform the inversion of the

5   basement geometry. Well data, seismic horizons and 2D gravity models were used to construct an initial model. The inversion process then applied consisted in isolating all the gravity contributors, i.e. different sources (sediments and regional component) and calculating their gravity response. That was then subtracted from the Bouguer gravity anomaly (BA) map (Figure 3).

10   Accordingly, the gravity model building for the inversion consisted of the following steps:

- Calculation and removal from the BA map of the gravity anomaly generated by the stratigraphic succession below 0 m (Figures 6a and 6c) assuming a constant density for each layer (table 1)

15   - Analysis, calculation and removal of the long wavelength/deep signal corresponding to the regional anomaly (Figure 6b and 6d)
- Generation of the basement topography by inverting the residual anomaly after subtracting the above-mentioned contributions (Figure 7).

The sedimentary succession was interpreted and modelled by Alcalde et al. (2014) using

20   a 3D seismic cube. Eight layers were used in order to characterize the signal of the sediments. Three of them, corresponding to the Cenomanian-Maastrichtian, Early Cenomanian (Utrillas Fm.) and Aptian-Albian (Escucha Fm.) layers lie above the sea level, and were used to compare the BA obtained using a reduction density of 2400 kgm^{-3} with that obtained using a model based on Alcalde et al., (2014). The latter map

25   had a higher wavelength number component that needed to be filtered out, worsening the resolution of the final results and accordingly, was discarded. The remaining five layers correspond, from shallower to deeper, to: Late Jurassic-Early Cretaceous Purbeck, Dogger, marly Lias, Lias limestones and Lower Jurassic Anhidrites.

The forward calculation of the sediments gravity anomaly was performed using a

30   constant density for each layer (table 1). To build the sedimentary model we used the five layers described above, down to the top of the anhidrites. To solve the ambiguity generated by the unknown depth of the base of the anhidrites we used the constraints

provided by the 2D gravity models and the seismic profile shown in figure 5a. These datasets support the use of a constant thickness (100 m) layer of anhidrites. Furthermore, the seismic profile presented by Alcalde et al. (2014) shows a general homogeneity in the thickness of the layers for the study area. A bottom imaginary

5   boundary for the Keuper rocks was used in order to avoid cutting the overlaying strata so no errors were carried into the inversion process. Finally, the long wavelength/deeper contribution to the BA was removed by using the simplest Butterworth filter.

Three cross-sections (Figure 5d) were extracted from the results of the gravity inversion. These include the sedimentary layers down to the anhidrites and the

10   basement. Two of them coincide with the location of the 2D gravimetric models, NE-SW and WNW-ESE (Figures 3 and 5a and c) and the third one in NW-SE direction. The cross-sections have been used to make a comparison with the previous 2D models and to assess the basement structure crossing the main tectonic features that are also highlighted by the derivatives (Figure 4c, d).

15   **4. Results from the microgravity data**

The BA map (Figure 3) shows negative values ranging between -53.2 and -48.5 mGal, which are characteristic of continental crust. It is portrayed by a minimum located in the west-central part of the survey area where two parallel rows of low values are identified with NW-SE direction. From there, the anomaly increases towards the south and the

20   north, suggesting a concave ENE-WSW direction structure, with maximum values found in the SE area. The gravity gradients found to the south of the minimum are strong.

The separation of the long and short wave-length components by upward continuation of the gravity field shows that the regional anomaly (Figure 4a) is characterized by an

25   E-W directed low in the central/northwestern area. This low shows values ranging between -52.6 mGal and -49 mGal, and it is bounded by highs to the SE and partly to the NW. The residual anomaly resulting from subtracting the regional anomaly to the Bouguer anomay map (Figure 4b) shows variations of 1.5 mGal. It is characterized by NW-SE lows located in the centre of the study area, and bounded by highs to the S and

30   NW. Furthermore, there is a strong gradient in the southern part of the map with an almost E-W direction.

The derivatives presented in Figure 4c and d aid in the interpretation of the structures affecting the Hontomín area. Above all, the gravity gradient existing to the south of the gravity dataset and already evidenced in Figures 3 and 4b, is clearly imaged by both derivatives. The vertical derivative shows, as does the residual map in Figure 4b, NW-

5   SE minima that appear to be cross-cut by an E-W maximum in the southern part of the map. The expression that these features have in the vertical derivatives map indicates *Explain* that they respond to shallow density contrasts.

The computed 2D models have mainly helped to capture the deep structure. They have shown to be more sensitive to the variations in the shallower layers and in the basement

10   topography than those in the mid sections of the sedimentary succession. These can be ~~assigned to be~~ due to the small differences in density of the Jurassic succession. Model 1 has a NE-SW direction (Fig.5a) and crosses the main structural features of the area, i.e. South and East Faults (Alcalde et al., 2014). Both faults are identified in the model to affect~~ing~~ the basement and the sedimentary succession. While the South Fault affects all

15   the sedimentary packages, the East Fault seems to be fossilized by the late Cretaceous sediments. The structural configuration of the profile shows a dome-like structure, with a thick layer (up to 2000 m) of Keuper evaporites. The Jurassic succession is affected by a minor fault that affects the lower Cretaceous as well.

Model 2 has an approximate E-W direction and crosses the East Fault (Fig. 5b). The

20   vertical offset of the East Fault is around 400 m, and it has a 45° dip. The basement in the western sector shows a progressive uplift. The dome-like structure is recognized in this model as well as in Model 1, and is represented by a growth of the Keuper evaporites thickness, forming a gentle fold on the overlaying succession.

The processing workflow applied to the BA data in order to perform the inversion of

25   basement topography has led to a series of maps presented in Figure 6. Figure 6a represents the gravity response of the sedimentary succession modelled by Alcalde et al. (2014). The forward calculation includes ~~from~~ the Cenozoic down to an internal boundary within the Keuper Rocks. Gravity minima are found to the SE of the study area and describes an irregular shape in the SE corner. It is in accordance with were the basement

30   appear to be deeper in the gravimetric models allowing a thicker Keuper layer. Maxima appear to the W and has a round shape. Another maxima appears situated in the centre where the basement is deeper in the gravimetric models. Figure 6b present the map of

the calculated long-wavelength filter and shows a gentle negative gradient towards the NW. The values have a range of less than 3 mGals. Given the reduced dimensions of the survey area it is difficult to discern the depth of the source we are filtering out. In any case, we believe it is related with density variations within the upper crust and

5   below the top of the basement, and it may be either compositional or structural.

The resulting final grid used to perform the inversion of the gravity data is that obtained from subtracting the regional contribution in figure 6c to the BA map without the sediments gravity signature (Figure 6b) down to an imaginary flat surface within the Keuper layer. This approach represents the most accurate that we could build to ensure

10   the best outcome of the gravity inversion and is shown in figure 6d. It shows again an E-W minimum in the central part reaching values of -2.1 mGal. Maxima appear once more in the SE corner of the area and reach values above 1.4 mGal. A strong E-W gradient exists again in the southern part of the study area. This map allows us to undertake the inversion of the geometry of the boundary giving that anomaly, i.e. the

15   top of the basement/base of the Keuper layer.

The inversion has been performed within the Geosoft platform, using GM-SYS 3D module. The initial setup consisted in a two layer model, the upper one formed by Keuper salts and the bottom one, by the basement. A mean density of 2520 kg·m^{-3}, which includes that of all the layers above the Keuper, even the ones located above sea

20   level, was used as background density. The results of inversion are shown in Figure 7a and picture a deep basement ranging roughly from -2000 m below sea level to -2650 m below sea level, with a mean depth of -2300 m. Its geometry shows a pair of lows in the central-west area slightly elongated in a NW direction and bounded at the NW and SE by highs. The lows lay parallel to a well-defined gradient zone that has been identified

25   in most of the gravity maps generated along this paper. According to its relevance, this feature seems to represent one of the main structural elements of the area, which according to its position, must be the South Fault (Alcalde et al., 2014, and Figure 5a).

The geometry of the top of the basement allows us to calculate that of the Triassic Keuper salts (Figure 7b) by calculating the space between the top of the basement and

30   the bottom of the anhydrites layer. They appear to have a mean thickness of 1660 m with a maximum of 2020 meters thick around the centre-east of the area. This is in agreement with the data derived from exploration well Rojas NE-1, near Hontomín,

where a total thickness of 1400 m was drilled (Carola et al., 2015). The borders of the area appear to be the location where the Triassic Keuper is the thinnest with values of about 1200 meters. In general, the thickness of the layer is conditioned by the mobility of the salt and the migration pathways generated by the tectonic events.

5   Three cross-sections (location in figure 3) presented in figure 5d were derived from the results of the inversion of the gravity data including the layers from the 3D seismic. Two of the cross sections coincide with the two 2D gravity models and show a relatively good correlation with them (Figures 5a and c). The third profile (Figure 5c), runs in a NW-SE direction and accounts for the NW basement high presented in the

10 basement map (Figure 7a). Cross-section 1 running in NE-SW direction show a good correlation with the 2D Model 1 and shows a deep basement affected by the South and East Faults and a thick Keuper layer overlaying it.

Finally, a THD has been applied to the residual gravity anomaly obtained from the Hontomin area (Figure 6d) and is presented in figure 8. Results of this process are

15 relevant to identify gradient zones and accordingly fault zones, and will be discussed in the next section.

5. Discussion

The outcome of the analysis of the high resolution BA map of the Hontomin area and its

20 integration with the 3D seismic results acquired over the same area (Alcalde et al., 2014) results in a coherent model of the structure of the dome that characterizes this area and sheds some light about its evolution. Even though a good agreement between gravity and seismic data exists regarding the topography of the basement, some issues remain unsolved in the NW sector of the area.

25 ### 5.1 Structural setting of the basement

The Hontomín dome has been described as an extensional forced fold (Tavani et al. 2013) originated by the extension and reactivation of Permo-Triassic normal faults affecting the basement. The presence of a detaching level represented by the Keuper Triassic salts produced the forced folding in the upper sedimentary cover by migration

30 of these salts (Tavani et al. 2013; Carola et al. 2015). For the area of study, Carola et al.

(2015) have suggested a thin-skinned configuration based on surface geology, well data and vintage seismic lines.

Here, we present a comprehensive model, from surface to basement, for the area of Hontomín centred in the surroundings of the spot where the CO_2 storage site is currently being developed. The new model suggests a local thick-skinned deformation style for the area with two major faults affecting the basement, namely the South and the East faults, already described by Alcalde et al., (2014). This model defines an area divided in three main blocks, south, centre-northwest and northeast.

The THD presented in Figure 8 delineates high gradient areas affecting the residual gravity dataset of Figure 6d. These zones are interpreted as faults (discontinuous lines in Figure 8) and are compared with the ones described by Alcalde et al. (2014). Among these, a ~E-W striking one stands out in the southern area and is interpreted as a major fault, coinciding with the South Fault as defined by Alcalde et al., (2014). Its gravity gradient is observed in most of the gravity maps produced in this paper, including the residual gravity map and derivatives shown in Figure 4 and derivatives shown in Figure 8, indicating that it affects sediments and basement. Furthermore, the cross-sections derived from the 3D model (Figure 5c) show an offset in the basement of 150 m for the South Fault. Another fault parallel to the South Fault is shown in figure 5a, close to the thickest point of the Keuper evaporites, and has a normal displacement of the basement and an offset of approximately 200 m. These two faults combined create a downward displacement of 350 m of the basement. The South fault is thought to be a branch of the right-lateral Ubierna Fault affecting the basement and all the stratigraphic succession and conditioning the structural setting of the area. This fault has been affected by two deformation stages: a Late Jurassic Early-Cretaceous extensional stage (Tavani & Muñoz 2012) and a later Cenozoic compression related with the formation of the Pyrenees. The kinematics and sedimentary history of this fault were interpreted by Alcalde et al. (2014). They suggest a flower-like structure associated with the strike-slip movement of the Ubierna faults. The Jurassic-Lower Cretaceous succession shows a thicker sedimentary record to the NW of the South Fault, suggesting a normal displacement of the hanging wall during this periodAnother fault interpreted from the map in Figure 8 is located to the NE, strikes NW-SE and is correlated with the East Fault of Alcalde et al., (2014). It affects the basement and all the sedimentary

succession up to the Cenozoic packages, which are not affected by it. It has two minor faults associated (Figure 8) that strike in the same direction but have less extension. The vertical motion of this fault was described as well by Alcalde et al. (2014). Here, a downward displacement of the SW block during the Jurassic has been assigned by the

5   information extracted from the exploration wells. The 3D model created after the inversion of the gravity data shows a SW dipping fault with normal sense of motion and offsets of around 400 meters, comparable to the offset accumulated by the southern faults. The East Fault, interpreted in the seismic dataset is not as clear in the derivatives of the BA data (Figures 4c and d), although is visible and clear in the residual maps

10   (Figure 4b), in the basement depth maps (Figures 7 and 9) and in the THD performed over the final anomaly grid used for the inversion (Figure 8). In general, the South and East faults seem to have been reactivated during the Jurassic-Lower Cretaceous extension generating a sunken basement block.

Figure 8 also shows the good agreement existing between the South and East Faults as

15   deduced from gravity and from 3D seismic data. Good correlation exists too between minor fractures associated to these faults, like an E-W fault located to the north of the South fault and interpreted from both datasets.

Finally, the two 2D transects modelled from the Bouguer Anomaly map (Figure 5a and b), both running over the one or two boreholes, Hontomin 1 and 2 show a similar set of

20   faults and the same reservoir dome-like structure. However, these models are hardly comparable at depth with the seismic lines, since the latest do not reach the basement level.

The faults interpreted in the central sunken block by Alcalde et al. (2014) are not clearly recognisable in the THD map, which shows an irregular anomaly pattern in the central

25   domain. This could be due to either the confinement of faulting within the cover succession or to the minor offsets associated with these faults not generating strong enough gradients to be recognised with this method.

5.2. Structural setting of the sedimentary cover

30   Another set of faults can be interpreted from the THD of the reduced BA map (Figure 8). These strike NNW-SSE and have limited length. Even though they have a weak

signature, they are similar to those interpreted from the seismic data striking in almost N-S direction (Alcalde et al., 2014) which were described as active during the Liasic period. However, there is a discrepancy regarding their area of influence as the latter were interpreted to be associated to a possible Triassic extensional normal faulting

5   affecting the basement that triggered the movement of the Triassic evaporates. However, they do not appear to affect the basement topography or its gravity signature (Figures 7, 8 and 9) except locally to the SW, or at least, they do not produce a basement offset identifiable in the gravity data. This suggests that this set of faults may only affect the Jurassic and Triassic succession and they can be associated with the

10 movement of the Triassic evaporites towards the basement wall causing the dome growth.

Despite the general good agreement between the basement model presented here and that presented by Alcalde et al. (2014), there are still some differences, especially concerning the NW sector. Here, the basement topography appears to be higher as

15 deduced from gravity data than in their seismic model. Four hypotheses can be proposed to explain this discrepancy (Figure 10). The first explanation (Figure 10a) is that this basement high deduced in this area by this gravity study is real. This basement high could be explained as a rollover anticline generated by the listric geometry of the South Fault. In Figure 11 this hypothesis was compared with a seismic profile from

20 Carola et al (2015). It shows a thickening of the pre-rift and evaporitic layers towards the NW. To accommodate this increase in thickness we propose that another normal fault has to be present somewhere outside our study area, affecting the basement with the hanging-wall dipping to the NW.

The remaining hypothesis imply that the gravity high observed in the NW sector is not

25 only produced by a basement high, but also by a complex organization of the stratigraphic succession. The second proposed hypothesis (Figure 10b) portraits a reduced Keuper thickness in this area, which would imply a general increase of the gravity signal. This could be explained as the result of the migration of the Keuper evaporties towards the dome and would imply a thickening of the Jurassic-Recent

30 statigraphic succession in this zone. Figure 10c shows a third possible scenario where the positive gravity anomaly is related to the occurrence of a dense stratigraphic unit, which could correspond to Triassic anhidrites laterally passing to the less dense Keuper

evaporites of the dome domain. The last hypothesis presented in this study (Figure 11d) portraits [shows] a very similar scenario although in this case, the lateral passage from Keuper evaporites to denser materials (i.e. gypsum.) would be the result of diagenetic processes associated with fluid circulation Nevertheless, we cannot rule out the possibility that

5   this structure is related to the edge effects generated after filtering an anomaly's regional component in such a small area.

The thickness of the Triassic salt layer in the Burgalesa Platform is very inhomogeneous from north to south. Exploration wells have drilled different thicknesses, ranging from 2000 m to just 300 m (Carola et al., 2015). Here, the average thickness of the Keuper

10   evaporites is 1660 m with maximum of 2020 m. This data evidences [These data provide evidence for] the mobilization of the evaporites towards the walls of the principal faults (South Fault and the East Fault), related to the migration pathways forced by the Cenozoic compressional stage (Tavani et al. 2013). This thickening is related to the gravity low observed in the BA map although it appears somehow displaced to the SE. Also, this configuration is clearly

15   pictured in the 2D models and the cross sections derived from 3D models (Figure 5).

6. Conclusions

The gravity analysis of the area of the Hontomín CO_2 storage site allowed us to further constrain the tectonic setting, basement geometry, faults relationships and Triassic salt

20   thickness of the area. The new basement model reveals a thick-skinned tectonic setting configured by two major faults. The South Fault affects the Paleozoic basement and all the stratigraphic succession above it, while the East Fault affects the basement and the sedimentary succession up to the Cenozoic sediments. We propose a half-graben like structure for the configuration of the South Fault. The basement high in the NW section

25   of the area, not affected by any structure, suggests that the South Fault may have acted as a listric fault configuring the basement topography in the NW sector.

Three sets of faults have been detected from the total horizontal derivative of the residual Bouguer Anomaly. All of these faults show a good correlation with those presented by Alcalde et al. (2014). The first two set of faults comprises the South Fault

30   and the East Fault respectively, which divide the area in three major blocks. These faults strike ENE-WSW and NW-SE and cover the entire area of study. Another set of NNW-

SSE direction faults has been interpreted. These faults have been related with another set of known faults affecting the basement; however, their gravity signature in the residual gravity map is not very conspicuous suggesting that they may affect just the Triassic Keuper evaporites and the Jurassic succession above but they do not affect the

5   basement or produce small offsets. Accordingly, they have been interpreted to be the result of the movement of the salt towards the main faults.

This paper shows the excellent results that integration of high resolution 3D gravity and seismic data produce. Overall, we have managed to build a consistent structural model for the Hontomín site from the topography down to the basement. The model relies on the integration of high resolution 3D gravity and seismic data.

10   **Acknowledgements**

We dedicate this paper to the memory of Prof. Andres Perez Estaún, who was a great and committed scientist, wonderful colleague and even better friend. The datasets in this work have been funded by Fundación Ciudad de la Energía (Spanish Government, www.ciuden.es) and by the European Union through the "European Energy Programme

15   for Recovery" and the Compostilla OXYCFB300 project. Dr. Juan Alcalde is currently funded by NERC grant NE/M007251/1. Simon Campbell and Samuel Cheyney are acknowledged for thoughtful comments on gravity inversion.

References

Alcalde, J., Marzán, I., Saura, E., Martí, D., Ayarza, P., Juhlin, C., Pérez-Estaún, A., Carbonell, R.: 3D geological characterization of the Hontomín CO2 storage site, Spain: Multidisciplinary approach from seismic, well-log and regional data. *Tectonophysics*. Available at: http://dx.doi.org/10.1016/j.tecto.2014.04.025. 2014.

Alcalde, J., Martí, D., Juhlin, C., Malehmir, A., Sopher, D., Saura, E., Marzán, I., Ayarza, P., Calahorrano, A., Pérez-Estaún, A., Carbonell, R.: 3-D reflection seismic imaging of the hontomín structure in the basque-cantabrian Basin (Spain). *Solid Earth*, 4(2), 481–496, 2013.

Alcalde, J., Martí, D., Calahorrano, A., Marzán, I., Ayarza, P., Carbonell, R., Juhlin, C., Pérez-Estaún, A.: Active seismic characterization experiments of the Hontomín research facility for geological storage of CO2, Spain. *International Journal of Greenhouse Gas Control*, 19, pp.785–795. Available at: http://dx.doi.org/10.1016/j.ijggc.2013.01.039, 2013.

Andrés, J.: Aplicación de la microgravimetría a la caracterización geológica del área de Hontomín (Burgos). MSc. Thesis, 2012

Blakely, R.J., Simpson, R.W.: Approximating edges of source bodies from magnetic or gravity anomalies. *Geophysics* 51, 1494–1498, 1986

Blakely, R.J.: Potential Theory in Gravity and Magnetic Applications, Cambridge University Press, Cambridge, 464 pp., DOI: 10.1017/ CBO9780511549816, 1995

Brown, R. N.: History of exploration and discovery of Morgan, Ramadan, and July oilfields, Gulf of Suez, Egypt, in: Facts and principles of world petroleum occurrence, edited by: Miall, A. D., *Canadian Society of Petroleum Geologists Memoir*, 6, 733–764, 1980.

Canal, J., Delgado, J., Falcón, I., Yang, Q., Juncosa, R., Barrientos, V. Injection of CO2-saturated water through a siliceous sandstone plug from the Hontomín test site (Spain): *Experiment and modelling. Environmental Science and Technology*, 47 (1), 159-167, 2013.

Carola, E., Muñoz, J.A. & Roca, E.: The transition from thick-skinned to thin-skinned tectonics in the Basque-Cantabrian Pyrenees: the Burgalesa Platform and

surroundings. *International Journal of Earth Sciences*. Available at: http://link.springer.com/10.1007/s00531-015-1177-z, 2015.

Chappell, A. R. and Kusznir, N. J: Three-dimensional gravity inversion for Moho depth at rifted continental margins incorporating a lithosphere thermal gravity anomaly correction. *Geophysical Journal International*, 174: 1–13. doi: 10.1111/j.1365-246X.2008.03803.x, 2008.

Contrucci, I., Matias, L., Moulin, M., Géli, L., Klingelhofer, F., Nouzé, H., Aslanian, D., Olivet, J-L., Réhault, J-P., and Sibuet, J. Deep structure of the West African continental margin (Congo, Zaire, Angola) between 5S and 8S, from reflection/refraction seismics and gravity data. *Geophysical Journal International*, *158*, 529–553, 2004.

Døssing, A., Hansen, T. M., Olesen, A. V., Hopper, J. R., & Funck, T.: Gravity inversion predicts the nature of the Amundsen Basin and its continental borderlands near Greenland. *Earth and Planetary Science Letters*, 408, 132-145. 10.1016/j.epsl.2014.10.011, 2014.

Elío, J., Nisi, B., Ortega, M.F., Mazadiego, L.F., Vaselli, O., Grandia, F. CO2 soil flux baseline at the Technological Development Plant for CO2 Injection at Hontomín (Burgos, Spain). *International Journal of Greenhouse Gas Control*, 18, 224-236, 2013.

Engen, Ø., Frazer, L. N., Wessel, P., and Faleide, J.I.: Prediction of sediment thickness in the Norwegian–Greenland 28 Sea from gravity inversion, *J. Geophys. Res.*, 111, doi:10.1029/2005JB003924, 2006.

European Union. Directive 2009/31/EC of the European Parliament and of the council of 23 April 2009 on the geological storage of carbon dioxide and amending Council Directive 85/337/EEC, European Parliament and Council Directives 2000/60/EC, 2001/80/EC, 2004/35/EC, 2006/12/EC, 2008/1/EC and Regulation (EC) No 1013/2006. 2009.

Filina, I., Delebo, N., Mohapatra, G., Coble, C., Harris, G., Layman, J., Strickler, M., and Blangy, J. Integration of seismic and gravity data - A case study from the western Gulf of Mexico. *Interpretation*, *3*(4), 99–106, 2015.
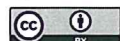
García-Mondejar, J.: Plate reconstruction of the Bay of Biscay. *Geology* 24, 635-638, 1996.

IEA Greenhouse Gas R&D Programme (IEA GHG), "CCS Site Characterisation Criteria", 2009/10, July 2009.

5 Jacobsen, B. H.: A case for upward continuation as a standard separation filter for potential-field maps: *Geophysics*, 52, 1138–1148, 1987.

Jacoby, W., and P.L. Smilde, Gravity Interpretation - Fundamentals and Application of Gravity Inversion and Geological Interpretation, Springer, Heidelberg, 2009.

Laubscher, H. P.: Die Sudostecke des Rheingrabens-ein kinematisches und 10 dynamisches problem, *Eclogae Geol. Helv.*, 75, 101–116, 1982.

Leveille, J. P., K. Larner, and J. Higgingbotham, A problem workshop: *The Leading Edge*, 24, 1126–1132, 2005. doi: 10.1190/1.2135107.

Manspeizer, W.: Chapter 3 - Triassic – Jurassic rifting and opening of the Atlantic: An overview, In: W. MANSPEIZER, Editor(s), *Developments in Geotectonics*, 15 Elsevier, 1988, Volume 22, Pages 41-79, ISSN 0419-0254, ISBN 9780444429032, http://dx.doi.org/10.1016/B978-0-444-42903-2.50008-7.

Nisi, B., Vaselli, O., Tassi, F., Elío, J., Delgado Huertas, A., Maadiego, L.P., Ortega, M.F. Hydrogeochemistry of surface and spring waters in the surroundings of the CO_2 injection site at Hontomín-Huermeces (Burgos, Spain). International Journal 20 of Greenhouse Gas Control, 14, 151-168, 2013.

Parker, R.L.: The rapid calculation of potential anomalies: *Geophysical Journal of the Royal Astronomical Society*, v.42:315-334, 1972.

Prado Pérez, J.A.R, Campos, C., Ruiz, M., Pelayo, F., Recreo, L., Lomba, A., Hurtado, S., Eguilior, L., Pérez del Villar.: Almacenamiento geológico de CO_2. Selección de 25 formaciones favorables. Comunicación técnica, Congreso Nacional del Medio Ambiente. Cumbre del desarrollo Sostenible. Madrid, 2008.

Pujalte, V., Robles, S., García-Ramos, J.C. and Hernández, J.M.: El Malm-Barremniense no marinos de la Cordillera Cantábrica. Geología de Espana. (J.A. Vera, Ed.), SGE-IGME, Madrid, 288-291, 2004.

Oldenburg, D. W.: The inversion and interpretation of gravity anomalies: *Geophysics*, 39, 526–536, 1974.

Ogaya, X., Ledo, J., Queralt, P., Marcuello, Á., & Quintà, A. (2013). First geoelectrical image of the subsurface of the Hontomín site (Spain) for CO2 geological storage: A magnetotelluric 2D characterization. *International Journal of Greenhouse Gas Control*, *13*, 168–179, 2013.

Ogaya, X., Queralt, P., Ledo, J., Marcuello, Á., Jones, A.G. Geoelectrical baseline model of the subsurface of the Hontomín site (Spain) for CO2 geological storage in a deep saline aquifer: a 3D magnetoteluric characterisation. *International Journal of Greenhouse Gas Control*, *27*, 120–138, 2014.

Quintá, A., and Tavani, S.: The foreland deformation in the south-western Basque-Cantabrian Belt (Spain). *Tectonophysics*, 576-577 (2012), 4-19, 2012.

Rousseau, J. H. L., Calandra, H., and de Hoop, M. V.: Three dimensional depth imaging with generalized screens: A salt body case study, *Geophysics*, 68, 1132–1139, 2003.

Rubio, F.M., Ayala, C., Gumiel, J.C., Rey, C. Caracterización mediante campo potencial y teledetección de la estructura geológica seleccionada para planta de desarrollo tecnológico de almacenamiento geológico de CO2 en Hontomín (Burgos). IGME- Instituto Geológico y Minero de España Technical Report, 182 pp, 2011.

Sava, P. and Biondi, B.: Wave-equation migration velocity analysis. II. Subsalt imaging examples, *Geophys. Prosp.*, 52, 607–623, 2004.

Serrano, A., and Martínez del Olmo, W.: Tectónica salina en el Dominio Cántabro-Navarro: evolución, edad y origen de las estructuras salinas. In: Ortí, F.& Salvany, J.M. (eds) Formaciones evaporíticas de la Cuenca del Ebro y cadenas periféricas, y de la zona de Levante. Nuevas Aportaciones y Guía de Superficie. Empresa Nacional De Residuos Radiactivos S.A., ENRESA-GPPG, Barcelona, 39-53, 1990.

Stadtler, C., Fichler, C., Hokstad, K., Myrlund, E. A., Wienecke, S., and Fotland, B. Improved salt imaging in a basin context by high resolution potential field data : Nordkapp Basin, Barents Sea. *Geophysical Prospecting*, (62), 615–630, 2014.

Tavani, S. et al.: Transpressive inversion of a Mesozoic extensional forced fold system with an intermediate décollement level in the Basque-Cantabrian Basin (Spain). *Tectonics*, 32(2), pp.146–158, 2013.

Tavani, S. and Muñoz, J.A.: Mesozoic rifting in the Basque-Cantabrian Basin (Spain): Inherited faults, transversal structures and stress perturbation. *Terra Nova*, 24(1), pp.70–76, 2012.

Tavani, S., Quintà, a. & Granado, P., 2011. Cenozoic right-lateral wrench tectonics in the Western Pyrenees (Spain): The Ubierna Fault System. *Tectonophysics*, 509(3-4), pp.238–253. Available at: http://dx.doi.org/10.1016/j.tecto.2011.06.013.

Vera, J.A.: Geología de Espa˜na. SGE-IGME, Madrid, p. 890, 2004.

Verduzco, B., Fairhead, J.D., Green, C.M., MacKenzie, C.: New insights into magnetic derivatives for structural mapping. *The Leading Edge*, 23(2), 116-119. 2004. doi: 10.1190/1.1651454

Vilamajó, E., Queralt, P., Ledo, J., and Marcuello, A. Feasibility of Monitoring the Hontomín (Burgos, Spain) CO2 Storage Site Using a Deep EM Source. *Surveys in Geophysics,* 34, pp. 441–461, 2013

Ziegler, P.A.: Evolution of the North Atlantic: An Overview. *AAPG Memoir*, 46, in A. J. Tankard, H.R. Balkwill Editors, Extensional Tectonics and Stratigraphy of the North Atlantic Margins, 111-129, 1988.

Table 1: Formation densities used in the gravity modelling and inversion of
5   microgravity data.

Age	Formation	Density (g/cm⁻³)
Cenozoic		2.33
Cretaceous		2.5
...	Top Utrillas+ Escucha Fm.	2.32
...	Top Weald.	2.34
...	Top Dogger+Purbeck	2.58
	Top marly Lias	2.62
	Top Limestones Lias	2.69
	Top Anhidrite	2.89
	Top Keuper	2.25
	Top Basement	2.75
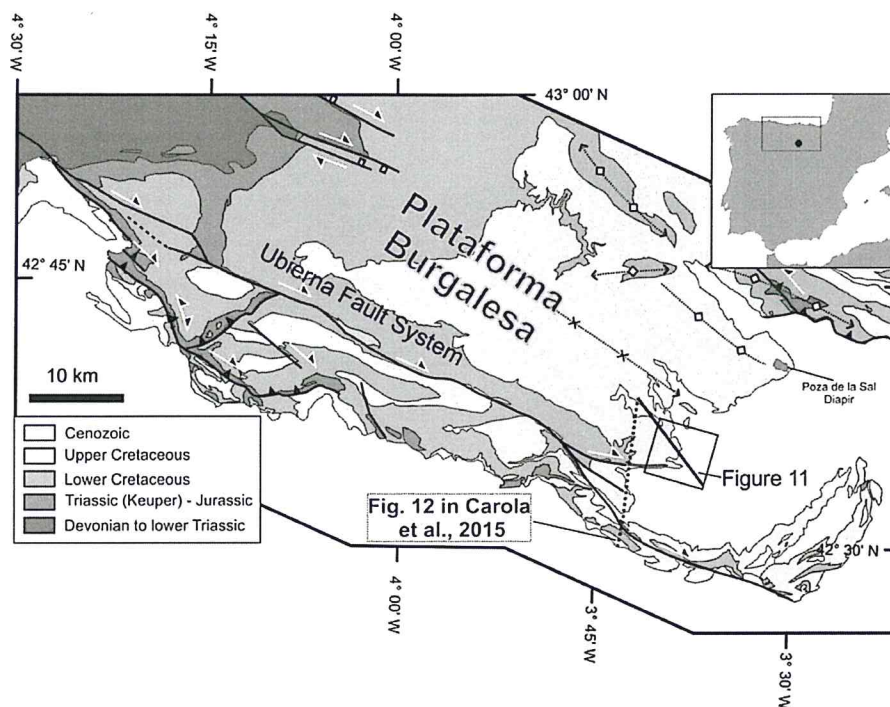
Figure 1: Location of the Hontomín site, black square, within the Burgalesa Platform (after Alcalde et al. (2014)). Bold line represent the position of the Figure 11.
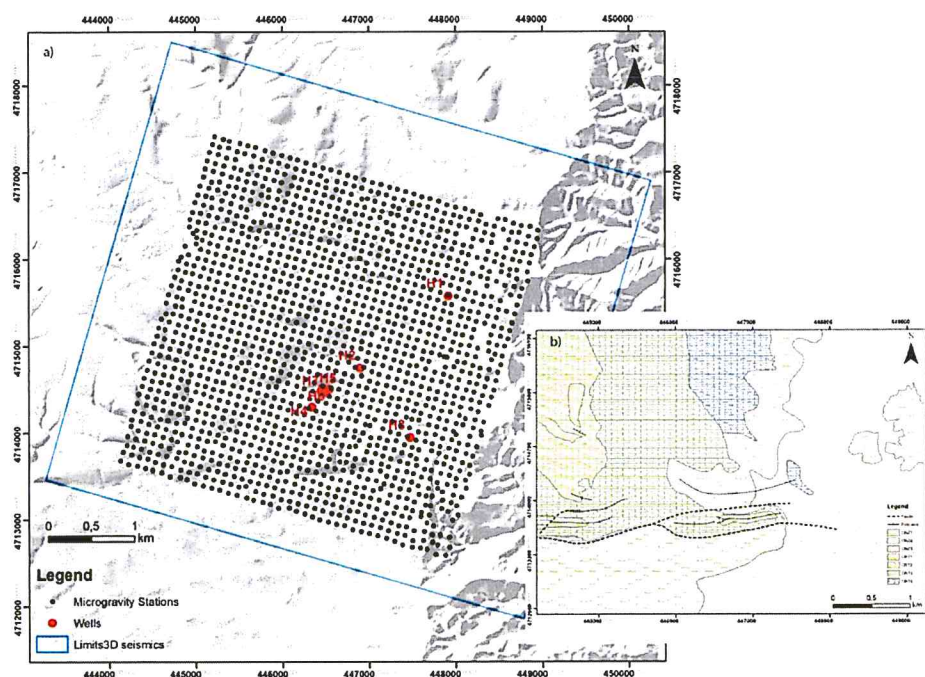
Figure 2: a) Location of the gravimetric stations (dark dots), boundaries of the 3D seismic experiment (blue line) and location of wells (red dots) and b) geological setting of the Hontomin site and the stratigraphic succession (Alcalde et al., 2014).
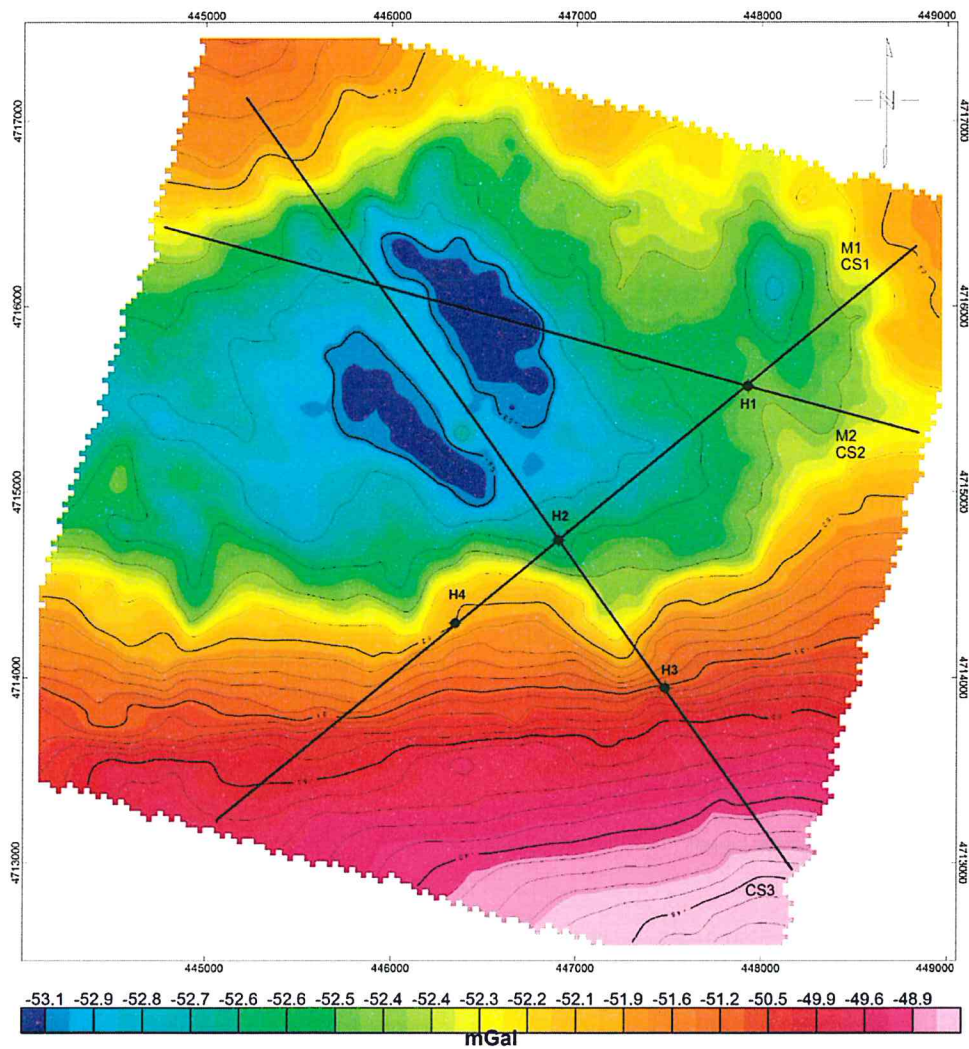
Figure 3: Bouguer anomaly map of the Hontomin area calculated with a reduction density of 2400 kg/m^3. Black dots mark the position of well data. Black lines represent the position of 2D models 1 and 2 and cross-sections (CS) 1-3 (Figure 5c) extracted from the final 3D model (Figure 7)
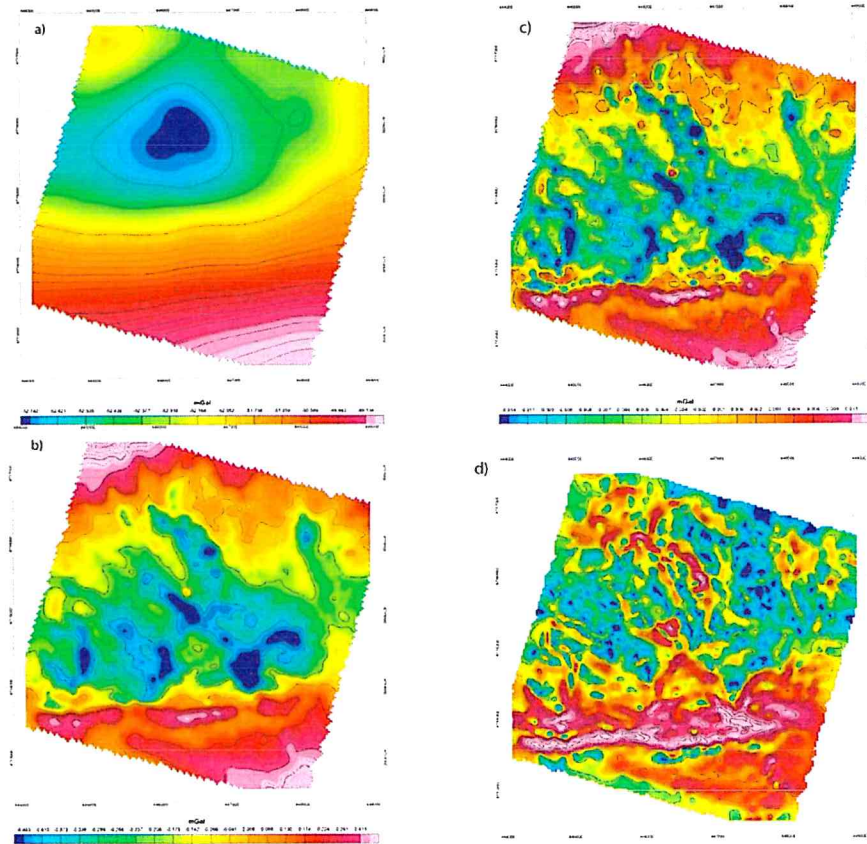
Figure 4: a) Regional gravity anomaly of the study area obtained by upward
continuation up to 350 m, b) resulting residual anomaly, c) first vertical derivative of
the Bouguer Anomaly (BA) map (order 0.75), d) total horizontal derivative (THD) of
the BA map
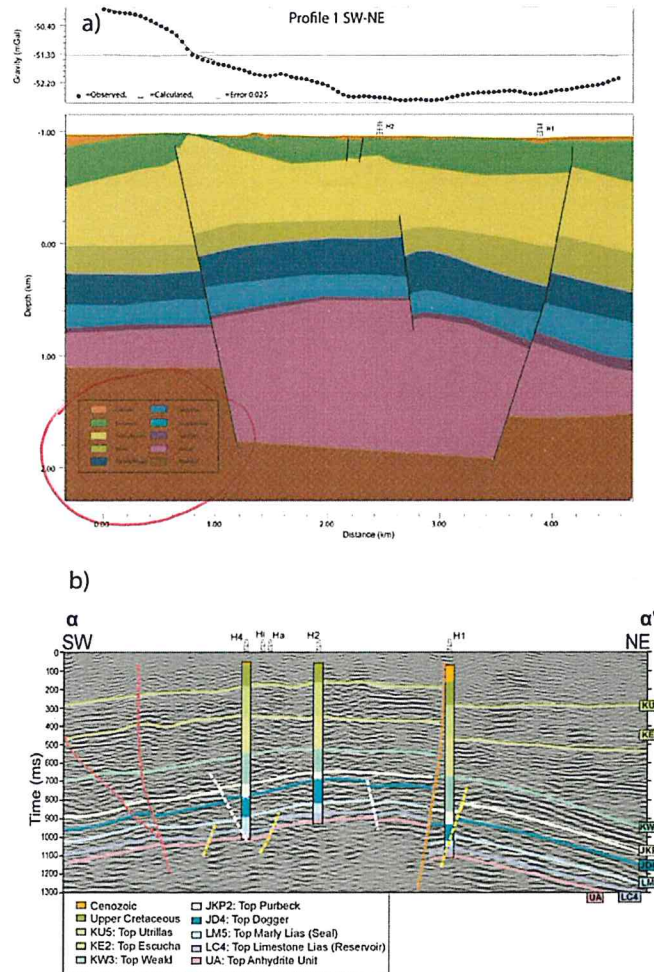
Figure 5: a) top: initial 2D gravity Model 1 and bottom: approximate corresponding two-way traveltime seismic section (after Alcalde et al., 2014) both sections are crossed by faults South and East (marked as bold lines in the figure). Offset along East Fault are opposite. The seismic section is interpreted down to the top of the anhydrite unit, marking the beginning of the evaporitic layers.
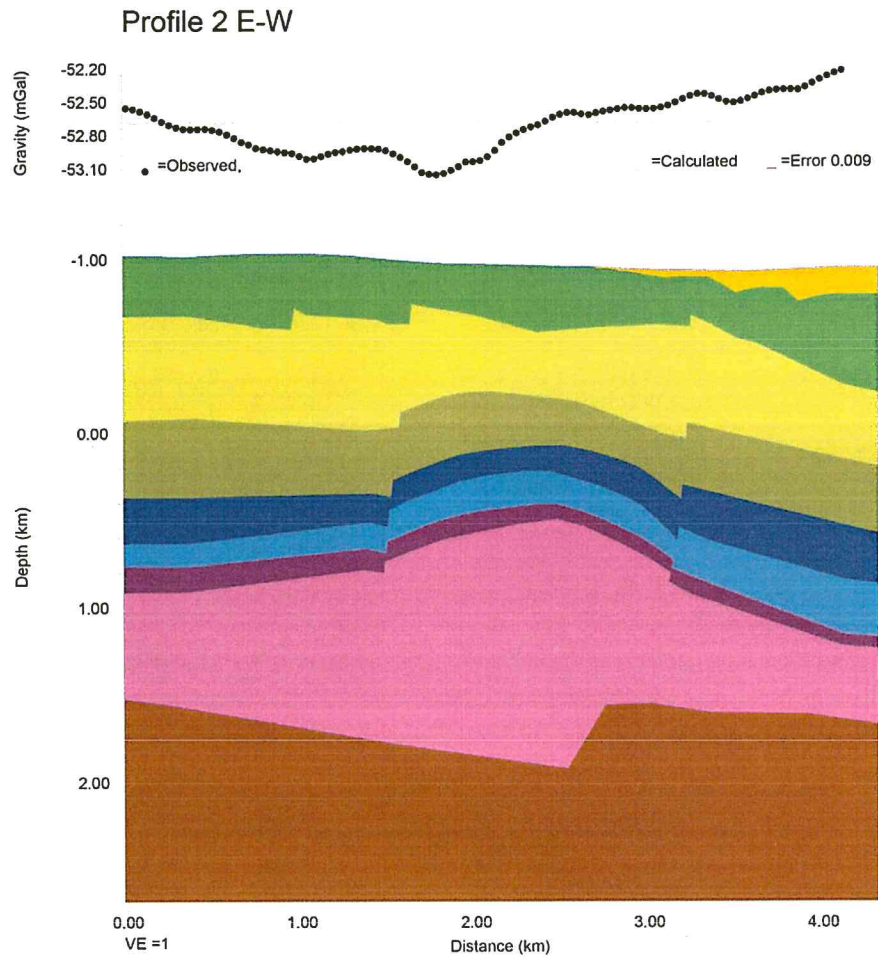
Figure5c: 2D gravity model striking in almost W-E direcction (see fig.3 for location)
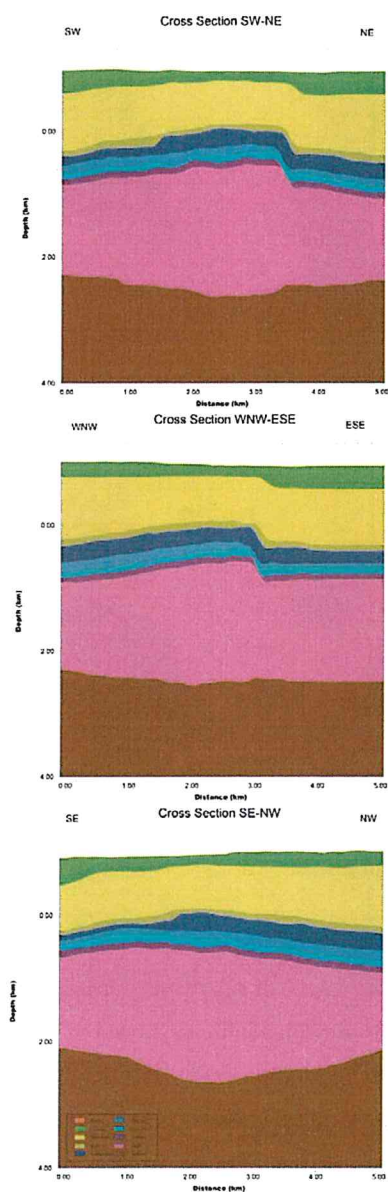
Figure 5d: Cross section extracted from the 3D gravity model of the basement (Figure 7a) generated integrating 3D seismics and microgravity inversion results (see figure 3 for location).
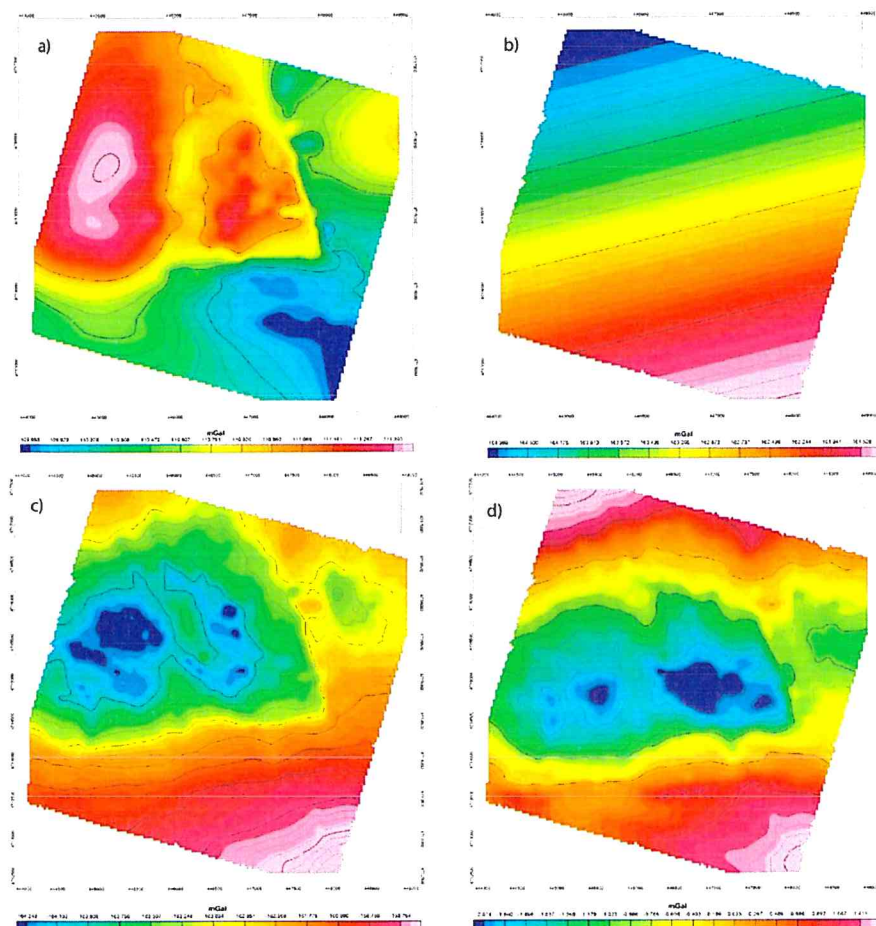
Figure 6: a) Gravity response of the sedimentary sequence as imaged by Alcalde et al. (2014) and by the 2D models presented in figure 5a and b; b) Regional component of the BA in figure 3; c) Gravity residual anomaly resulting from subtracting the map in figure 6a to the BA map in figure 3; and d) final anomaly grid resulting from subtracting the map in figure 5c to that in figure 5b. This grid will be the one used for inversion procedure.
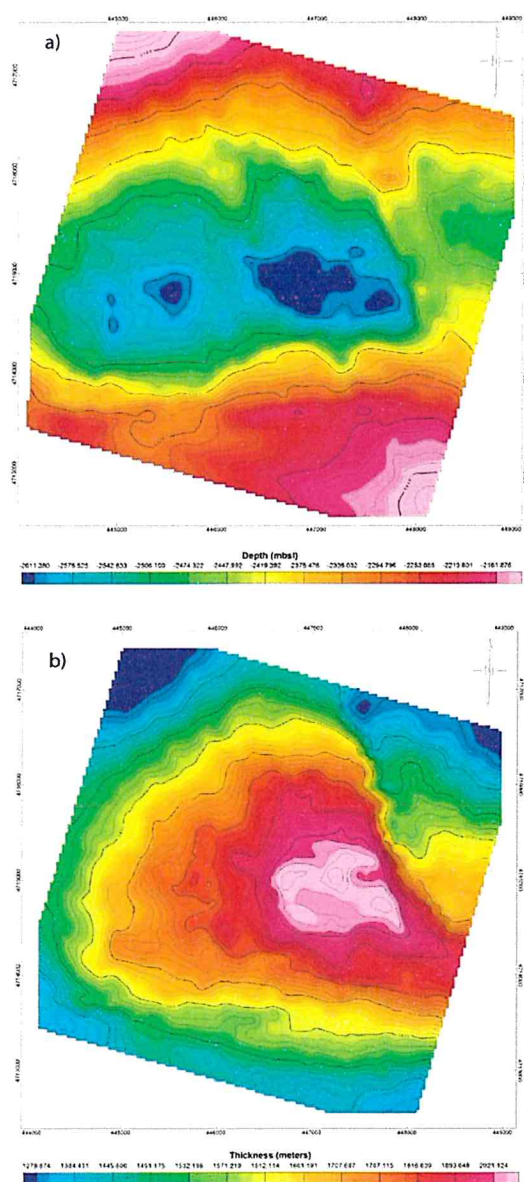
Figure 7: a) Basement topography derived from inversion of the residual gravity data
shown in figure 6d and b) thickness map of the Triassic Keuper evaporites after
comparing the basement topography and the bottom of the sedimentary sequence
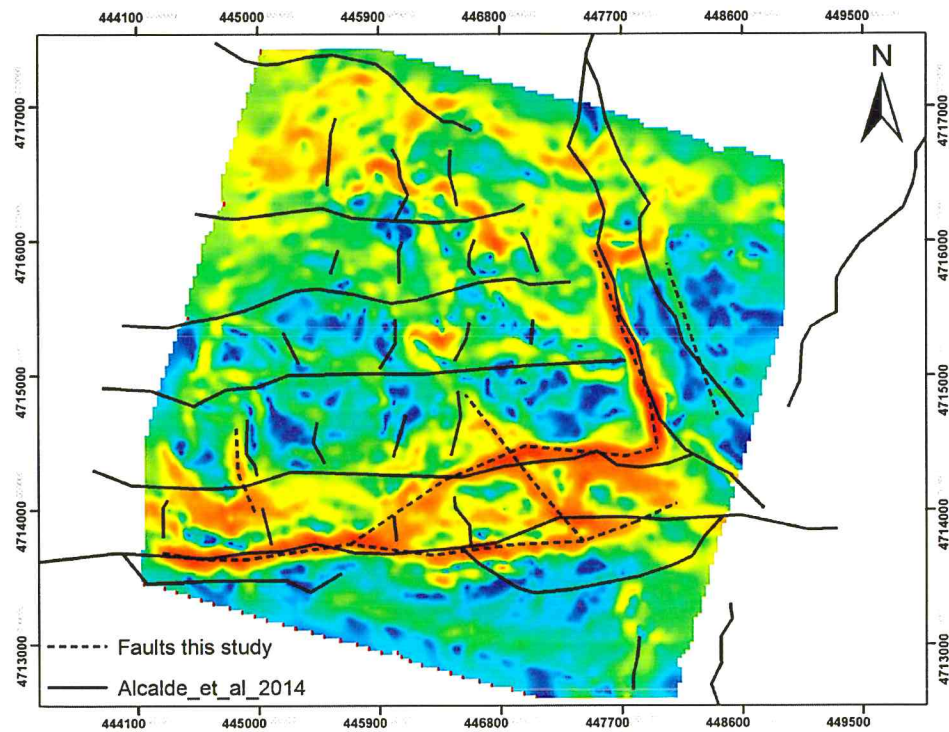
Figure 8: THD map of the gravity residual depicted in figure 6d with a comparison between the faults interpreted from this map and the gravity inversion (discontinuous line) and those interpreted by Alcalde et al. (2014) from 3D seismics.
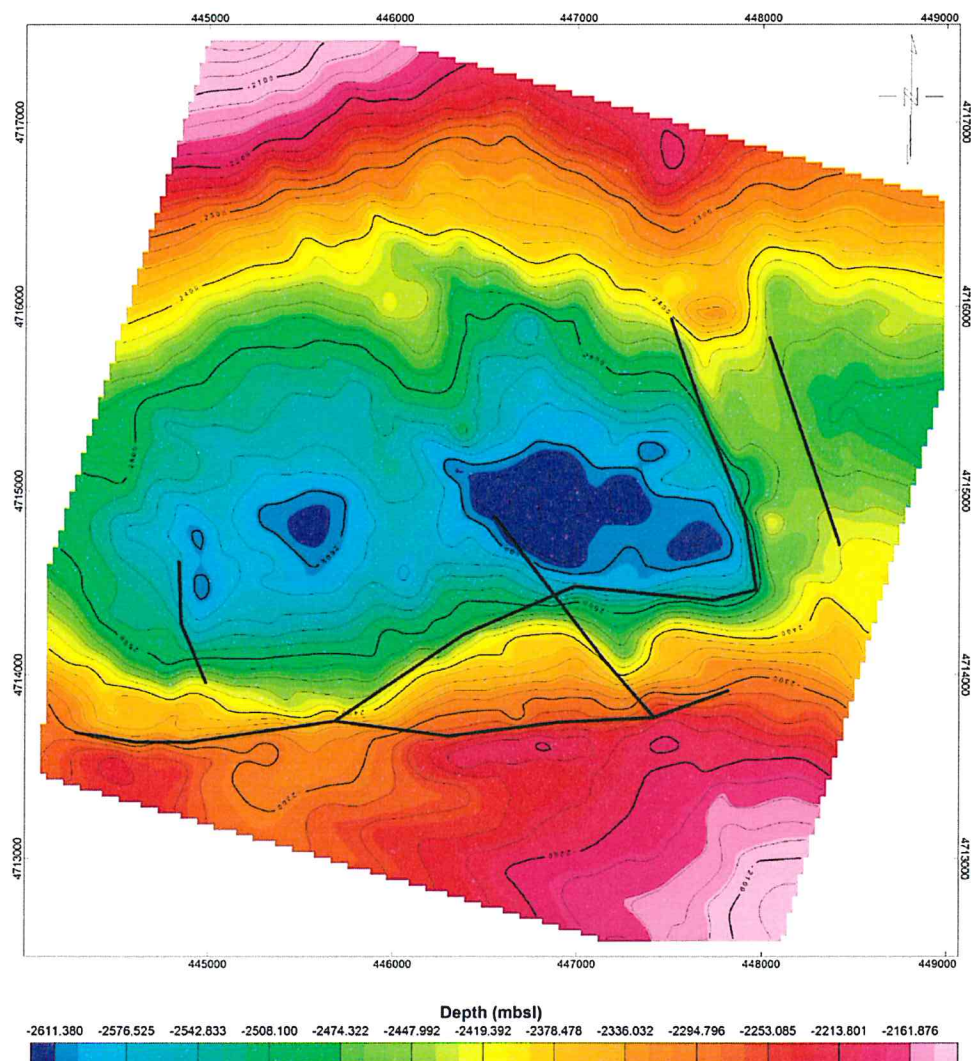
Figure 9: Faults interpreted from the THD of the residual gravity map and shown in

figure 8 superimposed on the basement topography map.
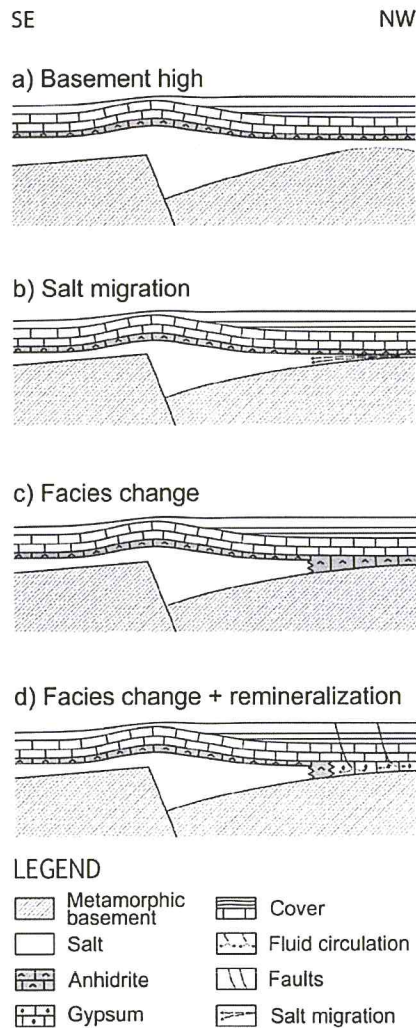
Figure 10: Schematic cross-sections in NW-SE direction, showing the different

5   possibilities to explain the discrepancy to the NW between the gravity model and that

presented by Alcalde et al (2014). a) Basement high, b) salt migration, c) facies change

from Keuper evaporites to anhidrites, d) facies change and remineralization of the

Keuper evaporites to gypsum.
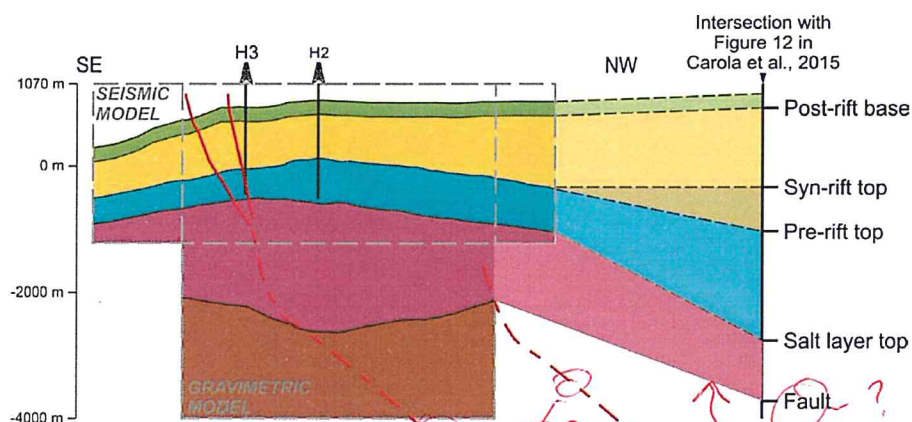
Figure 11. Correlation of the joint gravity and seismic model with that presented by
Carola et al (2015). There is a thickening of the pre-rift and the salt layers to the NW. A
new fault is proposed to accommodate the increased thickness.